An approach to calibrate the unsaturated hydraulic properties of a soil through numerical modelling of a small-scale slope model exposed to rainfall

L. Crescenzo - J. Peranić (*) - Ž. Arbanas - M. Calvello

https://orcid.org/0009-0004-4891-5020 - https://orcid.org/0000-0002-2574-6349 - https://orcid.org/0000-0002-5736-6746 - https://orcid.org/0000-0002-3899-1722

(*) corresponding author

L. Crescenzo - M. Calvello

Faculty of Civil Engineering

University of Salerno

Salerno 84084, Italy

J. Peranić - Ž. Arbanas

Faculty of Civil Engineering

University of Rijeka

Rijeka 51000, Croatia

E-mail: josip.peranic@gradri.uniri.hr

Abstract

Numerous studies have looked at rainfall infiltration as a triggering factor for rainfall-induced landslides. In addition to rainfall characteristics, soil hydraulic properties are recognized to play a crucial role in instability mechanisms. This study proposes a methodology for assessing the soil water characteristic curve and hydraulic conductivity function through finite-element seepage modelling of physical model tests. The approach is applied to an instrumented, small-scale slope model built with uniformly graded sand with a 30 degree inclination, exposed to homogeneous rainfall until the occurrence of failure. In a first stage, a sensitivity analysis is carried out to assess the influence of the Mualem-van Genuchten model parameters on the slope response. For this purpose, six physically based indicators are utilized to compare the numerical modelling results with the experimentally obtained data regarding the hydraulic response of the slope model. In the subsequent stage, a trial-and-error calibration stage is conducted to determine the set of parameters for which the difference between the numerically and experimentally acquired data is minimized. Ultimately, the suggested methodology facilitates the assessment of the optimal set of hydraulic parameters, to which both the sensitivity analysis and the trial-and-error calibration phase are anchored. The approach has demonstrated its effectiveness in calibrating the unsaturated hydraulic properties of the considered soil, as it properly addresses the physical mechanisms associated with rainfall infiltration in a slope.

Keywords: Rainfall infiltration, Landslide, Wetting front, Soil Water Characteristic Curve, Numerical modelling, Physical modelling

Introduction

As widely recognised, rainfall is one of the main triggering factors of both slow-moving and flow-like landslides [2, 47, 16, 38, 11, 10, 49, 44, 41, 61]. Indeed, the rainfall infiltration process can trigger a series of phenomena on a slope, potentially causing instability [69, 6, 45, 58], such as: i) decreasing matric suction; ii) increasing porewater pressures and rising of the groundwater level; iii) generation of destabilizing seepage forces; iv) increase in unit weight of soil due to increasing of water content. Many studies have been conducted to investigate the hydrological processes and the initiation mechanisms of landslides resulting from rainfall infiltration. Both field monitoring and experimental tests have shown that the unsaturated hydraulic properties of the soil layers very often play a fundamental role in these processes, clearly in combination with other important factors of the analysed boundary value problem, such as stratigraphy, soil types, slope inclination, and boundary conditions [73, 50, 17, 34, 53, 71, 68, 4, 9, 13, 46, 58].

Direct measurements of the unsaturated hydraulic parameters using traditional methods can be complex, time-consuming and not always effective, particularly when only data from laboratory tests are used. The Soil Water Characteristic Curve (SWCC), which relates soil suction to soil moisture content, is one of the most important features in unsaturated soil mechanics. Typically, a SWCC is highly nonlinear and relatively difficult to measure accurately [72, 54, 18] . While a wide range of soil suction, which fine-grained soils typically exhibit, requires the combination of different measurement techniques and devices [e.g. 59, 45, 48], measurements in uniformly graded coarse-grained soils, such as the material considered in this study, are often challenging due to a very steep and narrow SWCC where saturated and residual soil moisture conditions are typically separated by only a few kPa of matric suction [29, 57] . Depending on the measurement technique, equilibration times during suction measurements can vary from a few minutes to several months [63]. Moreover, not all measurement techniques and devices can provide a characterisation of the soil that is relevant for the process under consideration [28]. Hydraulic hysteresis or non-uniqueness in the functional relationship between soil water potential and water content is a well-known phenomenon that is characteristic of SWCC and has direct implications for hydraulic characterisation and hydraulic response modelling of unsaturated soils [72, 76]. The latter is reflected in the different pathways that the unsaturated soil undergoes depending on whether it is subjected to a drying or a wetting process. In general, for a given soil water potential, the soil tends to retain more water in a drying process than in a wetting process. To account for this, depending on the problem being considered, the main drying and wetting branches of a SWCC are usually determined in two different ways: i) the initially saturated soil is subjected to a drying process and measurements are conducted to define the main drying branch, or ii) measurements are made on an initially dry soil, i.e. with a moisture content close to residual conditions, which is subjected to a wetting process to obtain the main wetting branch [35, 28]. The Hydraulic Conductivity Function (HCF) provides a functional relationship between hydraulic conductivity and soil suction and, together with the SWCC, controls the seepage process in unsaturated soils. However, uncertainties and limitations in terms of prolonged testing times, expensive equipment, and limitations in measuring range make the determination of HCF through direct measurements very rare [e.g. 39, 19, 44]. To overcome these difficulties, many researchers have proposed different estimation methods or indirect methods to obtain the HCF of the soil [e.g. 21, 62, 35, 63, 70, 50].

Herein, a new methodology is defined aiming at calibrating the unsaturated hydraulic parameters of the soil in a slope subjected to rainfall, when monitoring data of soil water content are available. The procedure is applied and tested using a small-scale sandy slope exposed to a constant rainfall intensity and equipped with porewater pressure and soil moisture sensors at various locations. The proposed methodology and the obtained results are also used to investigate how the variation of each parameter defining the SWCC and the HCF of the soil affect the hydraulic response of a considered slope model. While previous studies have investigated how various factors affect the hydraulic response and stability conditions of slopes under rainfall infiltration conditions [e.g. 69, 59, 22], the results of the parametric analyses conducted in this study aim to guide and facilitate the calibration process. Although the test procedure could be modified to generalise its application, the methodology proposed here provides a hydraulic characterisation of soil undergoing wetting processes and is particularly well suited for the use with laboratory flume test results.

Rainfall infiltration in unsaturated soils

To understand the hydraulic mechanisms related to rainfall infiltration in soils, numerous approaches based on the advancement of the “wetting front” have been developed. The first model was proposed by Green-and Ampt (1911) [33], which describes the infiltration process through partially saturated soil. The model is based on Darcy’s law and makes the following simplifying assumptions: i) ponding condition at ground level; ii) homogeneous and isotropic soil; iii) sharp wetting front with fully saturated conditions above it and initial degree of saturation below it; iv) constant hydraulic conductivity of the soil, neglecting variations due to changes in moisture content. According to these hypotheses, the time necessary to saturate the soil, t_{sat}, to a depth z_{sat} is:

$$t_{sat} = \frac{S_{sat} - S_{in}}{k_{sat}} \left[z_{sat} - (h_p + C_c) \ \ln\left(\frac{h_p + C_c + z_{sat}}{h_p + C_c} \right) \right] \tag{1}$$

where S_{in} and S_{sat} are respectively the degree of saturation below and above the wetting front, k_{sat} is the saturated hydraulic conductivity of the soil, C_c is the capillarity coefficient, and h_p is the ponding head.

Several studies have been carried out to remove some of the limitations of the Green-Ampt model, considering layered soil stratigraphy [14, 15, 20] and time-dependent infiltration rate [27, 1]. However, most of the contributions keep the ponding condition at ground level, which may correspond to unrealistic precipitation rates for some soils. Very few studies have been carried out considering an infiltration rate lower than the saturated hydraulic conductivity of the soil, such as the one by Sun et al. (1998)[67], who identified the depth of the wetting front as:

$$z_w = \frac{(q_1 - q_0)}{n_s \left(S_{q_1} - S_{q_0}\right)} d \tag{2}$$

where d is the rainfall duration, q_0 is the surface flux at steady state condition (initial condition), q_1 is the water flux under transient conditions, n_s is the soil porosity, S_{q_0} is the initial degree of saturation in steady state conditions in equilibrium with the water flux q_0, and S_{q_1} is the degree of saturation corresponding to the depth z_w of the wetting front.

Considering the simplifying assumptions required to obtain an analytical solution, the conceptual wetting front model is not easily applicable to real cases. Instead, numerical methods enable the solution of the differential equation describing a transient groundwater flow (Richards, 1931 [62]) by properly schematizing any boundary value problem, thus considering, for instance, soil stratigraphy, heterogeneous initial conditions, time-dependent boundary conditions, and, most importantly, the non-linear hydraulic conductivity within partially saturated soils.

Indeed, the hydraulic soil behaviour in unsaturated conditions is highly dependent on matric suction, volumetric water content, and their variation over time. Several studies have been carried out to define the SWCC and the HCF characterising unsaturated soils, respectively differing for the number of parameters required and their applicability to different soil types [5, 15, 37, 16, among others]. One of the most frequently SWCC adopted in the literature is the van Genuchten model [30], which can be expressed in terms of the degree of saturation (S) as follows:

$$S = S_r + \frac{(S_{sat} - S_r)}{\left[1 + \left(\frac{h}{a}\right)^n\right]^m} \tag{3}$$

where h is the soil water potential, S_r is the residual degree of saturation, S_{sat} is the degree of saturation at fully saturated conditions, a and n are the fitting curve parameters related to an air-entry value and to the slope of the transition zone, respectively, with $m = 1 - 1/n$, as proposed by van Genuchten [51].

The dependence of the unsaturated hydraulic conductivity on the soil water content can be expressed as (van Genuchten, [51]):

$$k(S_e) = k_{sat}\, S_e^l \left[1 - \left(1 - S_e^{\frac{1}{m}}\right)^m\right]^2 \qquad \text{with} \qquad S_e = (S - S_r)/(S_{sat} - S_r) \tag{4}$$

where S_e is the effective degree of saturation, and l is an empirical constant.

The factor S_e^l was introduced by Burdine [8] and Fatt and Dykstra [24] to account for pore tortuosity and connectivity (Schaap and Leij [64]). Mualem [51] found out that l can assume both positive and negative value.

Theoretical framework for the model calibration using six control parameters

As already stated, the wetting front concept does not allow to consider many realistic stratigraphical settings, even relatively simple ones, such as the presence of an impermeable layer underlying a coarse-grained soil. Indeed, in this common stratigraphical condition for shallow rainfall-induced landslides, also a low intensity rainfall can initiate the saturation of the coarse soil layer, starting from the bottom boundary after the wetting front has reached it. To illustrate the hydraulic mechanisms that may occur with this stratigraphical setting yet neglecting, for explanatory reasons, the role of the slope angle, we can consider a soil column in one dimensional condition with a thickness T and an impervious boundary at the bottom (Fig. 1). Once the infiltration capacity drops to a constant value, it can be assumed that the amount of rainfall that can infiltrate the soil can be approximated by the saturated hydraulic conductivity (k_{sat}). In this sense, the value of the ratio between the rainfall intensity (q) and the saturated hydraulic conductivity (k_{sat}) allows us to distinguish between 2 types of saturation mechanisms: top-down saturation, for $q/ k_{sat} \geq 1$; and bottom-up saturation preceded by a downward wetting front propagation in unsaturated conditions, for $q/ k_{sat} < 1$ and the boundary conditions considered in the scheme.

In the first case (left side of Fig. 1), the rainfall produces a saturation mechanism from the ground level to the inner part of the soil column (Top-Down mechanism), which is in line with Green-Ampt conceptual model and can be expressed according to Eq. (1). The sharp wetting front fully saturates the soil, starting from the ground level, as time progresses (from t_1 to t_3). Tracing the degree of saturation in two points within the soil (A and B in Fig. 1), once the saturation conditions are reached, they remain unchanged until the end of the process, i.e., the complete saturation of the soil column. In terms of first derivative of the degree of saturation (S' hereafter), at any time the function assumes a null value until the wetting front reaches the point, then assumes an infinitive-value due to the "instantaneous" variation of the saturation condition, and then returns to a null value once a new equilibrium state is achieved. In the second case (right side of Fig. 1), when the rainfall intensity is lower than the saturated hydraulic conductivity of the soil, two phases are observable: a first one for which the increase of the degree of saturation, albeit not reaching fully saturated conditions, propagates downwards from the ground level to the inner zones of the soil, essentially following the behaviour described by the Green-Ampt model; a second Bottom-Up saturation mechanism that can be assimilated to a rapid upwards advancement of another wetting front, moving from the bottom boundary until the soil column is fully saturated. At any given point, right side of Fig. 1 shows that the initial conditions S_0 are kept until t_1, which is the time necessary for the rainwater to reach the point depth. Then the degree of saturation increases until time t_1^*, where a new constant “plateau” value (S_P) is reached and kept. Afterword the degree of saturation starts increasing again at time t_2, which corresponds to the arrival of the Bottom-Up mechanism, and then reaches its final value S_{sat} at time t_2^*, when fully saturated conditions are established at that depth. It is worth highlighting that in this scheme with an impervious bottom layer, the degree of saturation at the plateau S_P represents an apparent steady state condition, since it is kept constant until the upward saturation mechanism reaches the point of interest. The apparent steady state condition corresponds to a steady state condition in equilibrium with the rainfall applied only in the case of indefinite thickness of the permeable soil. In terms of S', the two phases are easily distinguishable considering the two peak values assumed by the rate of change of the degree of saturation. Of course, the time separating the two phases is dependent on the depth considered, and it decreases as the distance from the impervious layer decreases. The porewater pressures will behave in a similar way, keeping negative values during the first phase and then reaching positive values as soon as the second saturation mechanism reaches the point of interest.

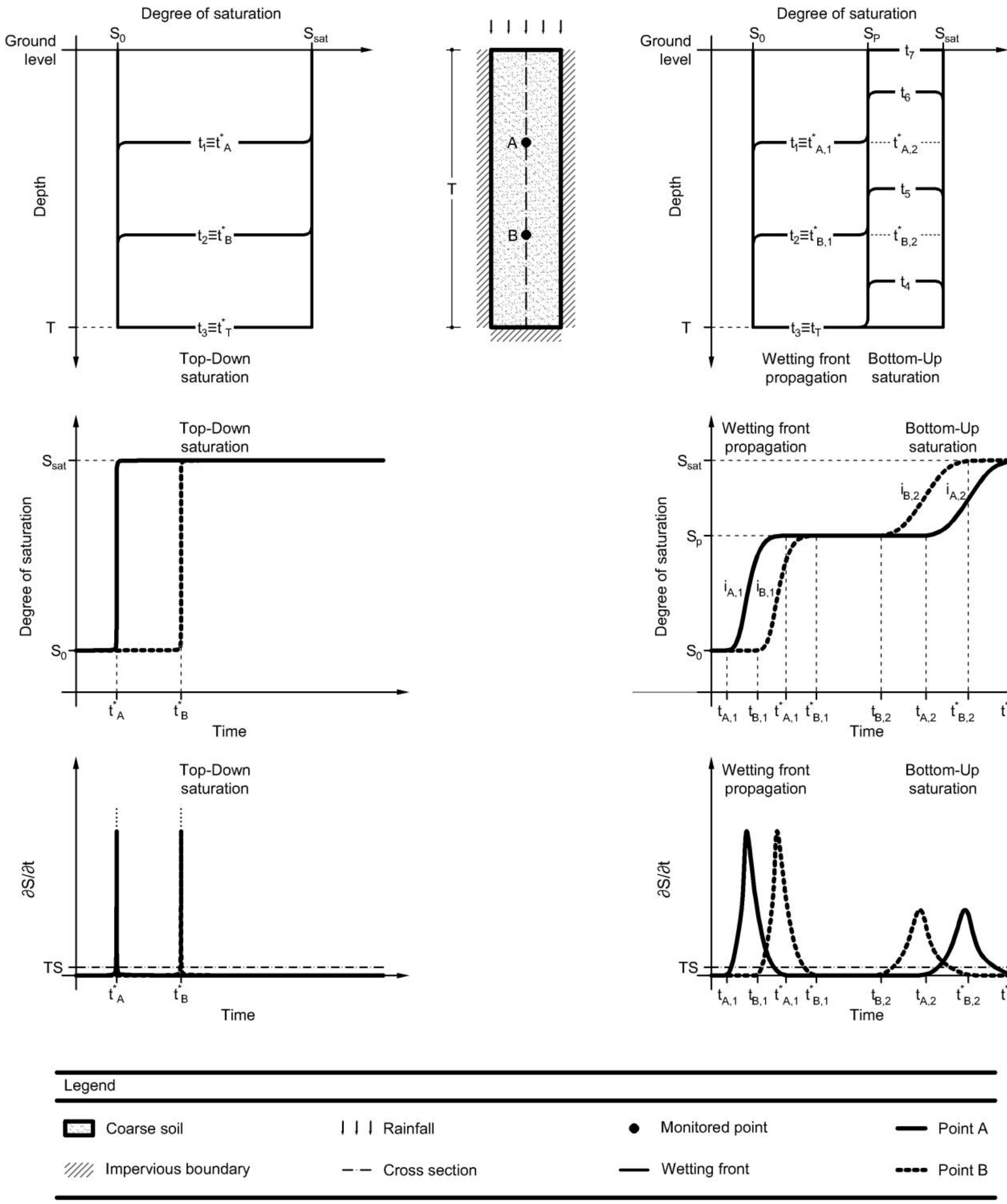

Fig. 1 Scheme of the saturation degree evolution in one-dimensional conditions at fixed times (first row in the figure) and over time at fixed depths (second and third row in the figure) for a coarse soil with a thickness of T over an impervious layer for: a) $q \geq k_{sat}$, i.e. top-down saturation (left side of the figure); b) and $q < k_{sat}$, i.e. bottom-up saturation preceded by a downward propagation of the wetting front in unsaturated conditions (right side of the figure)

Considering the two phases previously described for $q/k_{sat} < 1$, a downward propagation of the wetting front in unsaturated conditions followed by bottom-up saturation, it is possible to define some reference values for the time-dependent changes in the saturation degree at a given depth, which can be used as control parameters to evaluate the fit between the monitoring data, i.e. observations, and the results of a numerical model, i.e. predictions. At this scope, the following six parameters are considered: i) the initial degree of saturation, S_0; ii) the degree of saturation for the apparent steady state conditions, S_P; iii) the time of the initial change in the saturation degree, t_1; iv) the time to reach the fully saturated conditions, t_2^*; v) the average rate of change of the saturation degree for the wetting front advancement, i_1; vi) the average rate of change of the saturation degree for the bottom-up mechanism, i_2. The time derivative of the saturation degree is herein used to objectively define, by means of some threshold values (TS), the times at which the initial wetting front propagation and the bottom-up saturation start, t_1 and t_2, respectively, and come to an end, t_1^* and t_2^*, respectively, at the considered location. The case for $q/k_{sat} \geq 1$ can be considered a special case of the one described, for which only the following two control parameters can be defined: the initial degree of saturation, S_0, and the time at which the saturation degree abruptly changes from S_0 to S_{sat}, t^*.

In real cases, considering the many possible stratigraphical settings, slope geometries, rainfall characteristics and boundary conditions of a monitored site [12, 40, 25], it may not be straightforward to identify the above parameters, as the two phases may not fully develop where the monitoring points are located (e.g., shallow points at the top of a slope), or alternatively they may interact (e.g., points at the toe of a slope and close to the bottom boundary). Fig. 2 and Table 1 show how to correctly define the six control parameters in such cases, by depicting and considering four types of schematic trends (ST), defined as follows:

- ST0, when the Bottom-Up saturation mechanism fully develops;
- ST1, when only the wetting front propagation is present (which corresponds to the ideal case of infinite thickness of the soil);
- ST2, when the Bottom-Up saturation starts but does not fully saturate the soil (e.g., change in rainfall conditions);
- ST3, when the distinction between the first and the second phases is not clear (e.g., proximity of the monitored point to the lower boundary) and consequently the Bottom-Up mechanism shows its effect before the wetting front propagation phase is over.

While the scheme considered for the one-dimensional soil column can generally be considered representative and valid for analogous 2D or 3D slope problems, lateral seepage and water flow along the sloping bottom of the domain give rise to somewhat different conditions in the degree of saturation in different parts of the model. For example, the highest part of the slope may experience only the ST1 case due to lateral flow and gravity-induced seepage to lower parts of the domain.

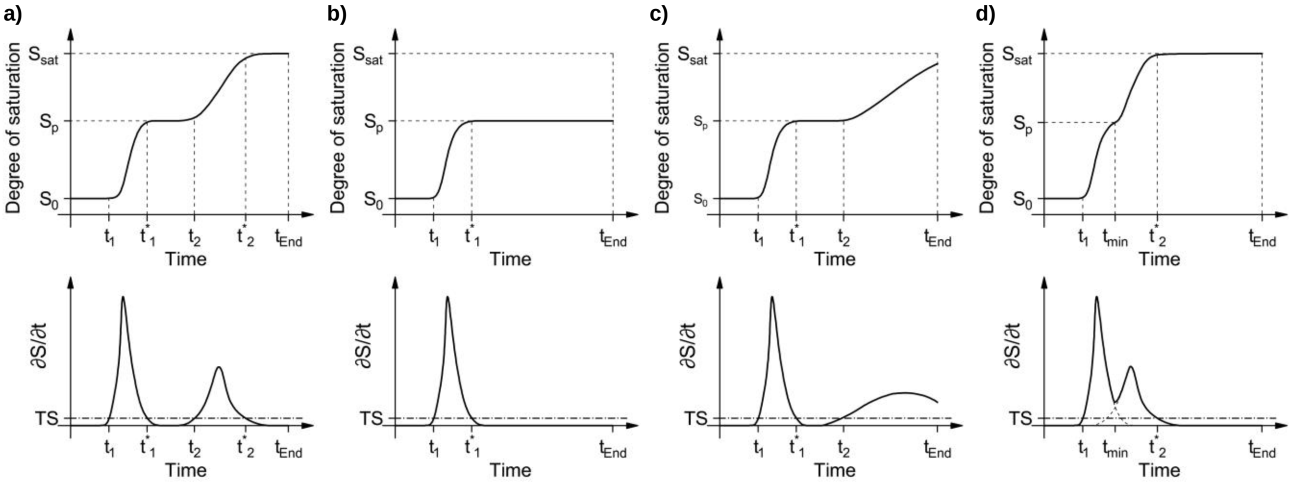

Fig. 2 Bottom-up saturation mechanism: a) ST0, mechanism completely developed (ideal situation); ST1, wetting front propagation only; c) ST2, bottom-up saturation initiated but not fully developed; d) ST3, wetting front propagation interacting with bottom-up saturation

Table 1 Computation of the six control parameters needed to calibrate a rainfall infiltration model for the four schematic trends identified in Fig. 2

Control parameter	Schematic Trend (ST)			
	0	1	2	3
Initial degree of saturation, S_0	S_0	S_0	S_0	S_0
Degree of saturation for the apparent steady state conditions, S_P	$\frac{1}{N}\sum_{i=t_1^*}^{t_2} S_i$	$\frac{1}{N}\sum_{i=t_1^*}^{t_{End}} S_i$	$\frac{1}{N}\sum_{i=t_1^*}^{t_2} S_i$	$S_{t_{min}}$
Time of initial change in saturation degree, t_1	t_1	t_1	t_1	t_1
Time of fully saturated conditions, t_2^*	t_2^*	-	-	t_2^*

Rate of change of saturation degree for downward wetting front propagation, i_1	$\frac{S_{t_1^*}-S_{t_1}}{t_1^*-t_1}$	$\frac{S_{t_1^*}-S_{t_1}}{t_1^*-t_1}$	$\frac{S_{t_1^*}-S_{t_1}}{t_1^*-t_1}$	$\frac{S_{t_{min}}-S_{t_1}}{t_{min}-t_1}$
Rate of change of saturation degree for bottom-up saturation, i_2	$\frac{S_{t_2^*}-S_{t_2}}{t_2^*-t_2}$	-	$\frac{S_{t_{End}}-S_{t_2}}{t_{End}-t_2}$	$\frac{S_{t_2^*}-S_{t_{min}}}{t_2^*-t_{min}}$

Case study: thoroughly monitored slope model built with uniformly graded sand

The small-scale slope model considered as a test case has been developed within the four-year research project “Physical modelling of landslide remediation constructions’ behaviour under static and seismic actions” (2018-2022) at the Faculty of Civil Engineering, University of Rijeka, Croatia. The platform for testing slope models exposed to various rainfall conditions under 1 g loading conditions is 1 m wide and consists of 3 main parts: the lower (L), the middle (M), and the upper part (H), which are 0.81, 1.43 and 0.31 m long, respectively. While the lower and upper parts were horizontal, the middle section was inclined at 30°. The slope was built from uniformly graded fine sand in strata of 6 cm with a total of 5 layers and compacted according to Ladd’s under-compaction method [39] to obtain a slope with a relative density of 50% and an initial gravimetric moisture content of 2%. The motivation for using clean sand in the study was to obtain a relatively uniform material for the laboratory tests, which would allow repeatability of the tests through the desired initial conditions in terms of target density or soil moisture content. Another consideration was that the soil with the basic properties reported in Table 2 undergoes negligible volumetric deformation when wetted, while its relatively high hydraulic conductivity ensures that all simulated rainfall infiltrates into the soil without causing surface runoff. These two aspects greatly simplify the interpretation of the results. During the model construction, i.e. after the compaction of each soil layer was completed, the soil moisture sensors TEROS 10 and TEROS 12 (METER Group AG, Munich, Germany), among others, were placed at the predefined locations and connected to data loggers, with the measuring interval set to 1 min. Once the entire model was completed and all sensors and monitoring equipment were installed, the slope model was subjected to a constant rainfall intensity of 79 mm/h. The rainfall intensity used in the study did not consider any specific rainfall event but resulted from the following requirements: no surface runoff should occur during the rainfall simulation, the working pressures in the rainfall simulator should ensure uniform coverage of the entire model, and the impact velocities of the raindrops should not cause surface erosion. These conditions were achieved using 3 axial flow full-cone spray nozzles at a working pressure of 2 bar, mounted 80 cm above the ground level and aligned to ensure uniform rainfall conditions in the model. The platform is also equipped with three drainage lines located on the front Plexiglas sidewall, allowing control of the water level in the lower part of the model. All drainage lines were kept closed until the groundwater level reached the surface of the model at the bottom of the slope, 79 min after the rainfall simulation began. Then the upper drainage line was opened to prevent the water level from rising further and to keep the groundwater in the lowest part of the model at the level of the model surface until the end of the test. Continuously collected data on changes in soil moisture, interpreted using the manufacturer’s generic calibration equation, and occasional readings from analogue tensiometers installed in the upper part of the model provided information on the hydraulic response of the model, while the optical 3D measurement system ARAMIS (GOM mbH; Braunschweig, Germany) and MEMS accelerometers monitored any surface or movements within the model. More details on the flume, model build-up procedure, the rainfall simulator and monitoring sensor network can be found in [55] and [57].

Table 2 Property of the soil used for the small-scale physical model

Parameter			Value
Specific gravity	G_s	(-)	2.7
Particle size	D_{10}	(mm)	0.19
Particle size	D_{60}	(mm)	0.37
Uniformity coefficient	CU	(-)	1.95
Minimum void ratio	e_{min}	(-)	0.64
Maximum void ratio	e_{max}	(-)	0.91
Saturated hydraulic conductivity	k_{sat}	(m/s)	1.6e-4
Initial porosity	$n_{s,i}$	(-)	0.44
Initial relative density	$D_{r,i}$	(%)	50
Initial gravimetric water content	w_i	(%)	2

Fig. 3 shows the main characteristics of the physical and numerical models, including the construction stages of the slope, the monitored points equipped with soil moisture (H6, H18, M6, M12, M18, M24, L6, L12, L18, L24) and porewater pressure (T5, T15, T25) sensors, the simulated rainfall conditions and the boundary conditions. Based on the negligible volumetric deformations observed during the 120-minute rainfall simulation, the numerical uncoupled single-phase groundwater flow analyses have been implemented adopting the commercial finite element software Plaxis2D [5]. The numerical model consists of 3649 15-noded triangular elements and 29767 nodes. The size of the mesh elements varies between 0.3704e-3 m^2 and 0.047e-3 m^2, while the hydraulic properties of the soil were described with the model of van Genuchten (1980) [30] and an isotropic hydraulic conductivity was assumed. All boundaries except for the ground level are set as impervious for a duration of 79 mins. For the later period of the numerical simulation, the first 6 cm of the bottom vertical boundary is set as a seepage area (Fig. 3) to allow water to drain from the model, which is consistent with the previously described opening of the upper drainage line to prevent the water table in the lower part of the physical model from rising above the ground level. A homogeneous rainfall with an intensity of 79 mm/h (i.e., 2.2e-05 m/s) was applied along the ground level of the domain for the entire duration of the analysis (120 min). The rainfall boundary condition is applied as a normal component of intensity in relation to the ground surface.

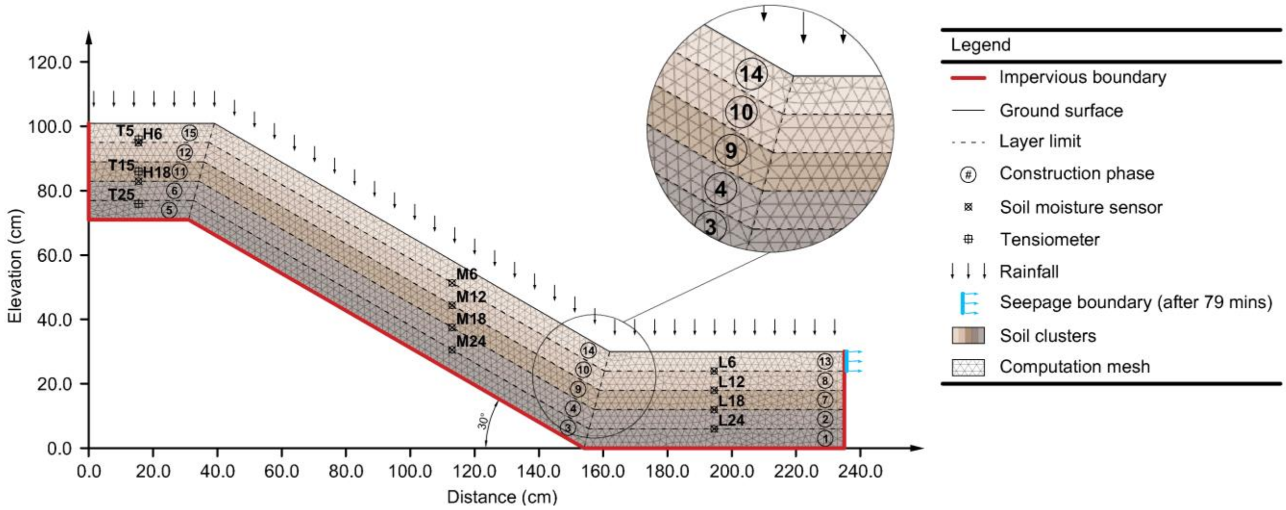

Fig. 3 Main characteristics of the physical and numerical models: stratigraphical and stage construction settings, monitored points, and boundary conditions assumed for the numerical analysis

The results of the physical model in terms of S are reported in the Fig. 4a,b,c,d. In addition, Fig. 4e,f,g,h show the first derivative of S, S', over the time where the Top-Down wetting front and Bottom-Up saturation mechanisms are clearly distinguishable. Generally, the first peak is higher than the second one for all the points monitored, indicating that the Top-Down wetting front is usually sharper than the Bottom-Up saturation. Moreover, the amplitude of the first peak is smaller than that of the second one, implying that the wetting front advancement is exhausted faster than the saturation one. This evidence is also visible in S curves, even if it is not easy to assess. Furthermore, for point L24 in Fig. 4d, is noticeable that the Top-Down wetting front is not totally exhausted when the upward saturation mechanism initiates and reaches the L24 point (ST3 saturation mechanism in Fig. 2d). In terms of S', once a threshold value has been assigned, the times t_1, t_1^*, t_2, and t_2^* can be easily computed. The value of the threshold to be considered depends on the data available, soil properties, and boundary conditions. In this study, a threshold value of 0.5 has been considered adequate. Once the timing has been assessed, the control parameters are evaluated as reported in Table 1 for each ST.

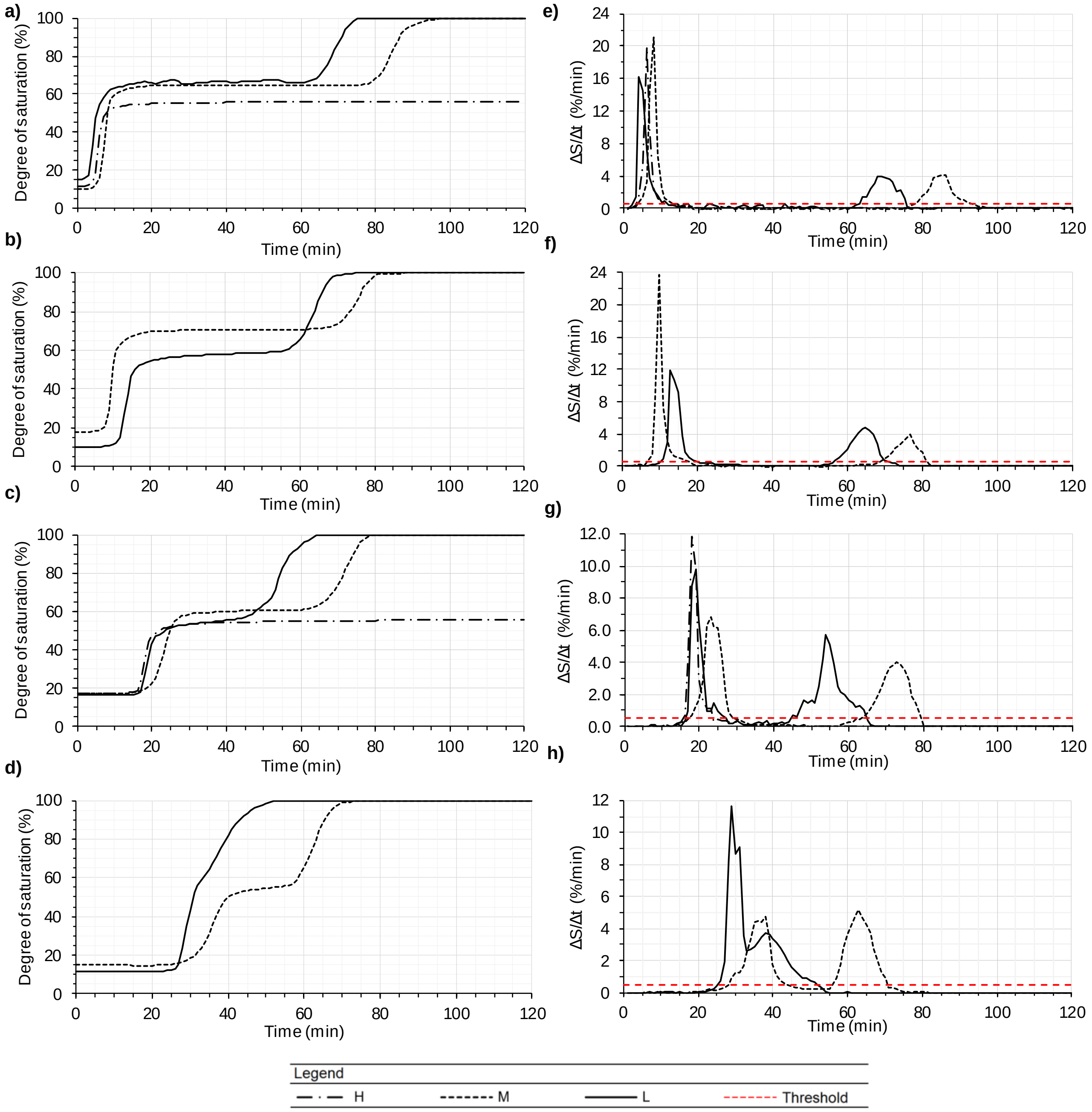

Fig. 4 Measurements of the physical model at the monitored points in the lower part (L, in continuous line), in the middle part (M, in dashed line) and in the upper part (H, in dot-dashed line) in terms of: saturation degree at depths 6 cm (a), 12 cm (b), 18 cm (c), 24 cm (d) from ground level, and corresponding prime derivatives at depths 6 cm (e), 12 cm (f), 18 cm (g), 24 cm (h) from ground level with threshold used to identify control parameters t_1, t_1^*, t_2, and t_2^* (see also Fig. 2)

Results and discussions

Initialisation of the numerical model

In the first numerical simulation, a homogeneous slope in terms of soil properties and initial degree of saturation has been considered. The hydraulic properties of the soil used for this analysis are those given as 'base case' in Table 3. In this case, as shown in Fig. 5, the degree of saturation is constant and equal to 10% for all the points monitored (green lines), but slightly distant from the actual conditions observed in the physical model (black lines). Therefore, a calibration procedure was applied in a second numerical simulation to obtain more realistic initial conditions for the moisture distribution in the numerical model (orange lines), i.e. conditions similar to those observed in the experiment. Indeed, knowing the volumetric water content in correspondence of each sensor and the measured values of volumetric water content under saturated conditions, it is possible to define an initial degree of saturation for each layer of the slope. The final result is a heterogeneous slope in terms of initial soil moisture distribution, but a homogeneous one in terms of porosity. Fig. 5 shows the effect of the initial soil moisture distribution on the numerical response in terms of the degree of saturation evolution over time. A higher initial degree of saturation speeds up both the initial downward wetting front propagation and the Bottom-Up saturation due to: i) higher values of unsaturated hydraulic conductivity; ii) a reduced rainwater storage capacity of the soil. However, the S_P value remained unaltered, indicating that these conditions are only correlated with the q/k_{sat} ratio and soil properties. This evidence is in line with Sun et al. [67] and highlights the importance of a correct assumption for the initial conditions. Indeed, it is clear from Eq. (2) that the initial degree of saturation can speed up the wetting front advancement and consequently the general response of the slope.

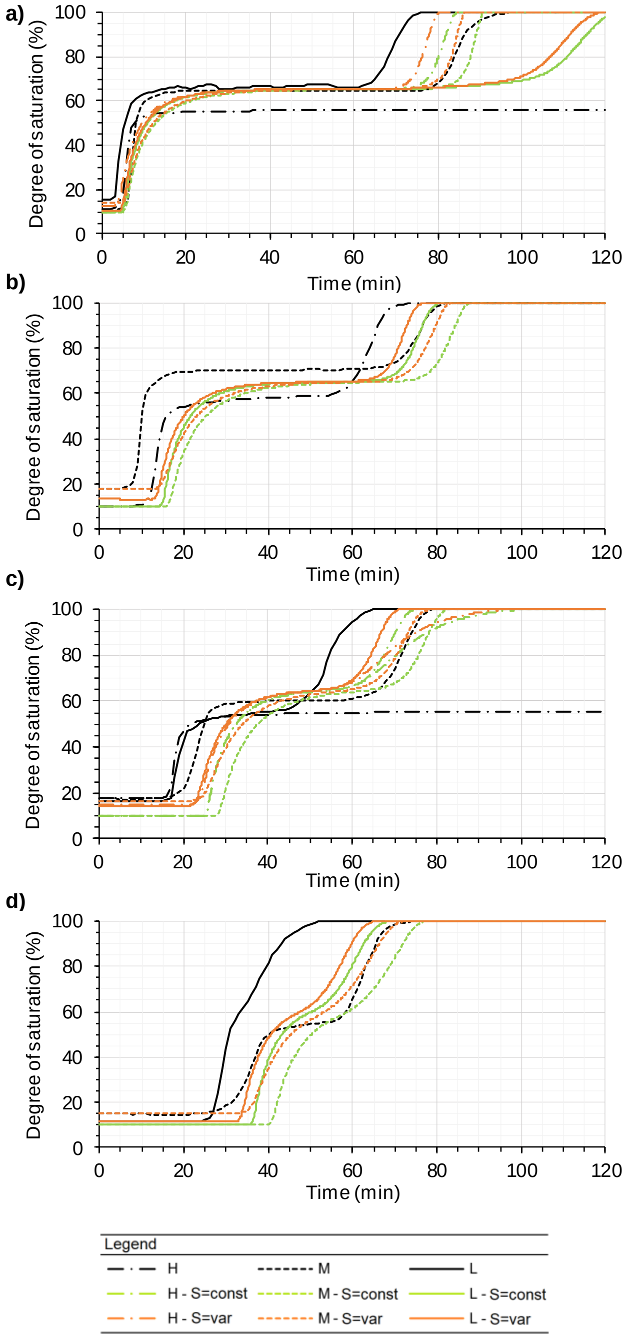

Fig. 5 Effect of the initial saturation degree for the monitored points in the lower part (L, in continuous line), in the middle part (M, in dashed line), and in the upper part (H, in dot-dashed line) in terms of the saturation degree at depths 6 cm (a), 12 cm (b), 18 cm (c), 24 cm (d) from ground level

Parametric analysis

To evaluate the sensitivity of the results to changes in the unsaturated hydraulic properties of the sand used in the small-scale slope, a parametric analysis has been carried out considering 4 parameters: n, a, l, and k_{sat} (Table 3). The base case (NM_BC) is characterized by a set of parameters usually valid for this kind of soil [31, 37] whereas the saturated hydraulic conductivity was determined from the constant head laboratory test results. In the other cases (NM_xx) the four parameters were varied once at the time, while keeping the other three constant to the preassigned basic values. The ranges of values of the unsaturated hydraulic parameters adopted in this parametric analysis are the following:

- n from 2.1 to 4.8;
- a from 1.96 kPa to 0.49 kPa (closely approximating the range of air-entry value [42, 26] ;
- l from -1.0 to 0.5, where the latter value is usually adopted without any distinction between the different soils and unsaturated hydraulic properties [51];
- k_{sat} from $5.0 \cdot 10^{-5} m/s$ to $3.3 \cdot 10^{-4} m/s$ (equivalent to $180\ mm/h$ to $1188\ mm/h$, respectively).

In particular, the upper limit of a and n parameters of the SWCC were estimated using the pedotransfer function based on the D_{60} and CU values of the sand used to build the physical slope model according to Benson et al [3]. The upper limit of the k_{sat} was derived by the D_{10} value according to Hazen [26].

Table 3 Values of the unsaturated hydraulic properties used in the different cases (NM_xx) of the parametric analysis

		Base case	Changing a			Changing n			Changing l			Changing k		
	ID: NM_	BC	a2.0	a0.7	a0.5	n2.1	n3.9	n4.8	l-1.0	l-0.5	l0.5	k5.0	k10.0	k32.5
Parameters	S_r (%)	5	5	5	5	5	5	5	5	5	5	5	5	5
	S_{sat} (%)	100	100	100	100	100	100	100	100	100	100	100	100	100
	a (kPa)	0.98	1.96#	0.65	0.49	10	10	10	10	10	10	10	10	10
	n (-)	3.0	3.0	3.0	3.0	2.1	3.9	4.8#	3.0	3.0	3.0	3.0	3.0	3.0
	l (-)	0.0	0.0	0.0	0.0	0.0	0.0	0.0	-1.0	-0.5	0.5§	0.0	0.0	0.0
	k_{sat} ($x10^{-5}$ m/s)	1.6	1.6	1.6	1.6	1.6	1.6	1.6	1.6	1.6	1.6	5.0	10.0	32.5*

#Benson et al. [3], § Mualem [51], * Hazen [32]

Effect of parameter “a”

Fig. 6 shows the SWCC and the HCF for the cases examined, indicating that decreasing of the air-entry value (a parameter) leads to a decrease of saturation degree at assigned suction and a corresponding decrease of the relative conductivity. Fig. 7 shows the response of the numerical model when the a parameter is varied. For increasing values of a, there is a faster downward propagation of the wetting front (t_1 decrease) and a slower Bottom-Up saturation (t_2^* increase). As the depth increases, these two phases tend to be closer to each other, and for the highest value of a sometimes they are indistinguishable (i.e., middle and lower parts for $a = 1.96$ kPa). Moreover, the steeper change in S for lower values of a suggests a wetting front advancement that, albeit slower, lasts a shorter time (greater t_1 with smaller t_1^*). The apparent steady state degree of saturation is not significantly affected by this parameter, as all the saturation time series tend towards to the same S_P value.

With respect to the initial porewater pressure, the strong dependence on a parameter is evident from Fig. 6, as the change in a causes the shift in SWCC. Consequently, assigning an initial degree of saturation corresponds to assigning an initial porewater pressure that increases as a decreases.

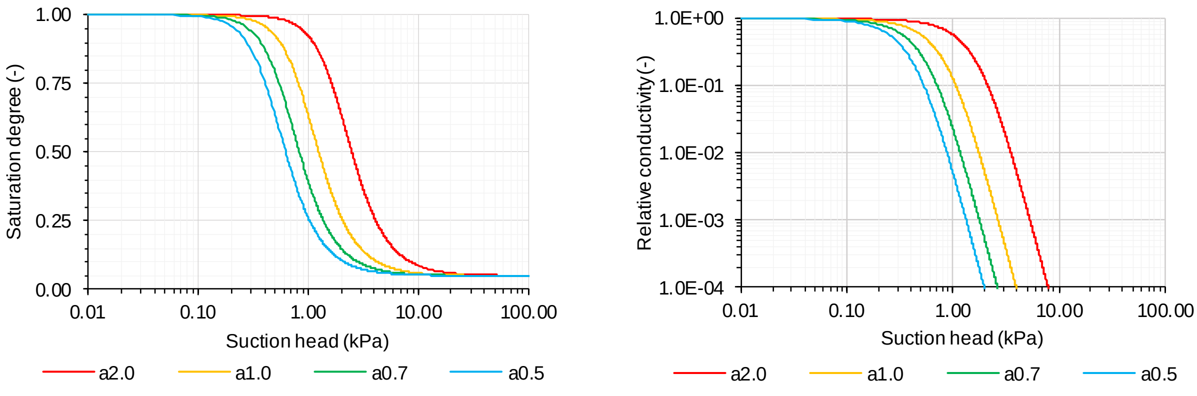

Fig. 6 SWCC (left) and HCF (right) for the values of the “a” parameter adopted in the parametric analysis

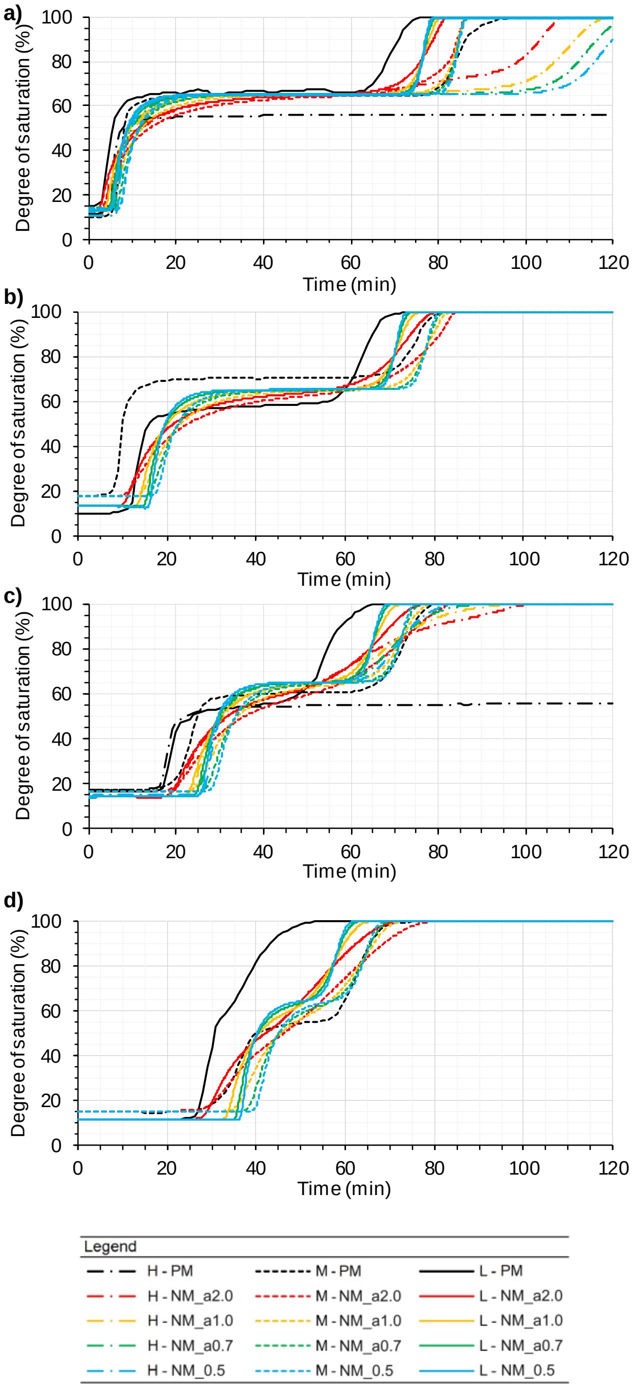

Fig. 7 Effect of the variation of the "*a*" parameter for the monitored points in the lower part (L, in continuous line), in the middle part (M, in dashed line), and in the upper part (H, in dot-dashed line) in terms of saturation degree at depths 6 cm (a), 12 cm (b), 18 cm (c), 24 cm (d) from ground level. [Legend: PM=Physical model, NM_xx=Numerical model case xx (see Table 3)]

Effect of parameter "n"

The n parameter represents the slope of the SWCC. In this study, four values for n have been considered, ranging from 2.1 to 4.8, with a base value of 3.0. This parameter has two different effects in relation to the value of suction (Fig. 8). At very low suction, an increase in n leads to higher values of saturation degree and relative conductivity in the SWCC and HCF respectively. In contrast, for higher suction values, the degree of saturation decreases with increasing of n and, consequently, the relative conductivity also decreases.

As for the model response, different values of n have the following effects (Fig. 9):

- Decreasing values of n produce a delay in the downward wetting front propagation at all depths, although more noticeable for deeper points. Similar statements are valid also for the Bottom-Up saturation.

- For decreasing values of n, higher S_P values are obtained. This can be explained by looking at the HCF for relatively low suction values (i.e. comprises between 0.0 to 1.0 kPa, in the range of values present in the slope after the wetting front passes and before the Bottom-Up saturation reaches the observed point), corresponding to lower relative conductivity and thus to a higher water accumulation during the wetting front propagation.

- In terms of the degree of saturation curve's gradient, lower values of n lead to smaller values of both i_1 and i_2, with the Bottom-Up saturation more significantly affected.

With regard to the initial porewater pressure, a similar statement can be made for the parameter n as for the parameter a. In this case, a decrease in the slope of the SWCC for decreasing values of n can be observed in Fig. 8, which corresponds to an increase in the initial porewater pressure for a fixed initial degree of saturation (values around 0.15).

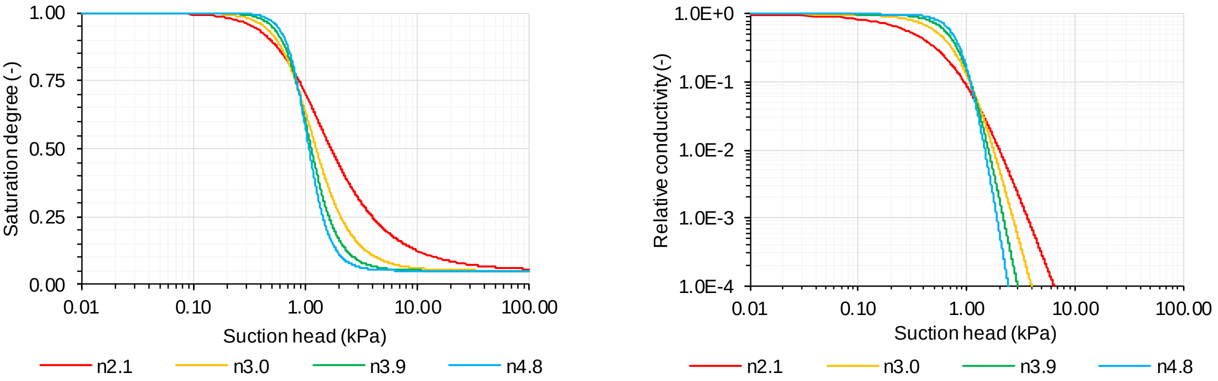

Fig. 8 SWCC (left) and HCF (right) for the values of the *n* parameter adopted in the parametric analysis

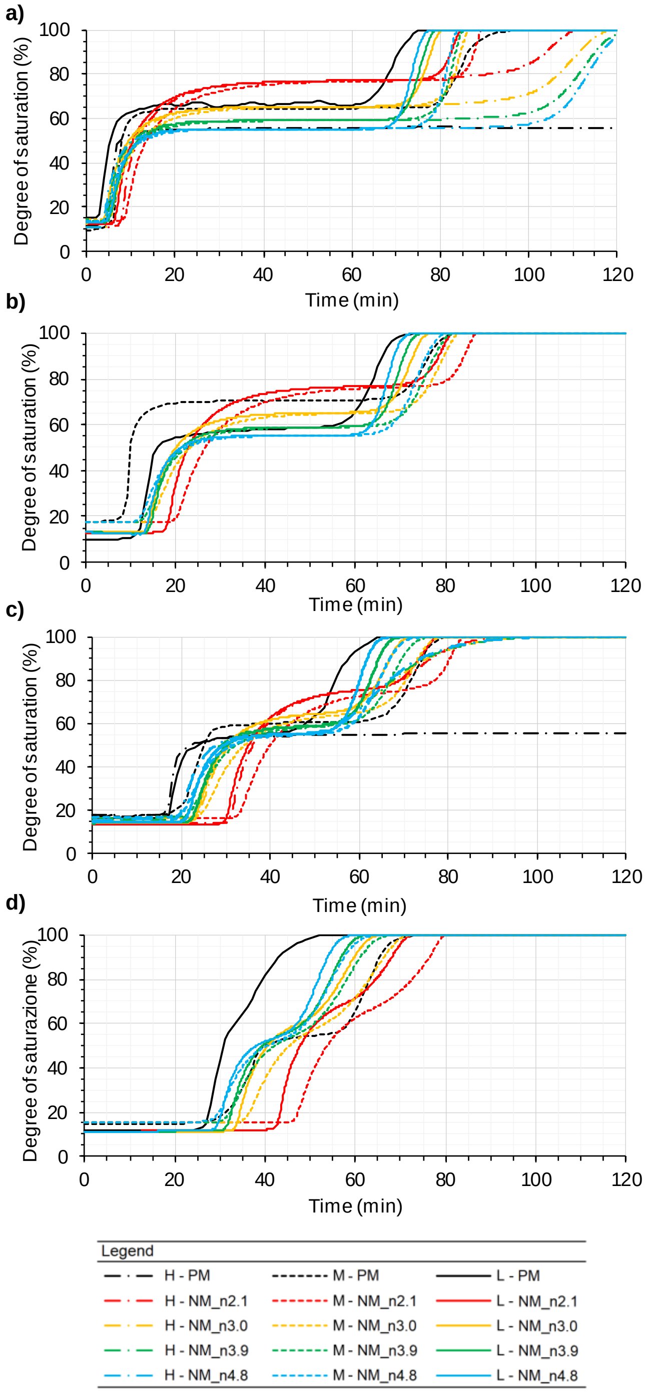

Fig. 9 Effect of the variation of the *n* parameter for the monitored points in the lower part (L, in continuous line), in the medium part (M, in dashed line), and in the higher part (H, in dot-dashed line) in terms of saturation degree at depths 6 cm (a), 12 cm (b), 18 cm (c), 24 cm (d) from ground level. [Legend: PM=Physical model, NM_xx=Numerical model case xx (see Table 3)]

Effect of parameter “l”

According to Eq. (3) and Eq. (4), the l parameter does not influence the SWCC, but only the HCF. Fig. 10 shows the effect of this parameter on the hydraulic conductivity, revealing that decreasing values of l imply an increase of the relative conductivity.

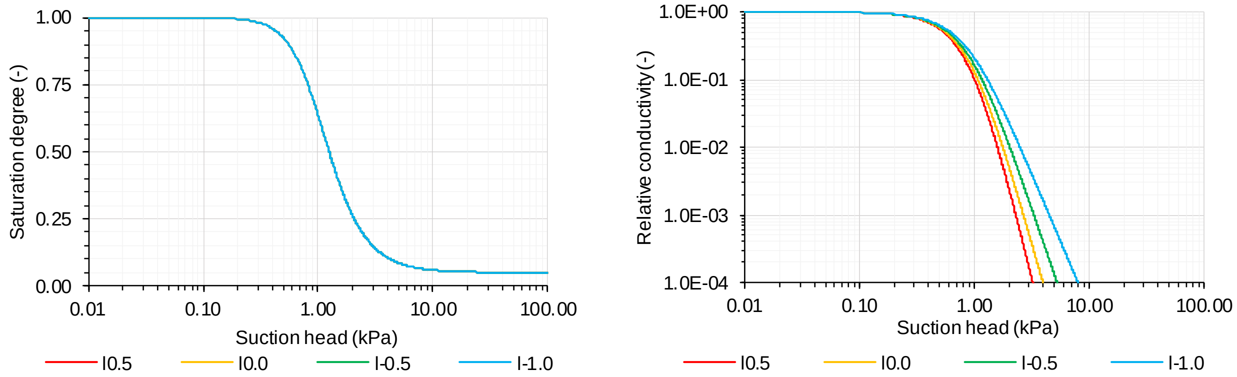

Fig. 10 SWCC (left) and HCF (right) for the values of the *l* parameter adopted in the parametric analysis

This parameter does not significantly affect the initial and final state but acts on the timing for reaching the apparent steady state conditions (Fig. 11). Specifically, for increasing values of l, there is a delay in the changes of the saturation degree due to a lower unsaturated hydraulic conductivity, which decreases the velocity of the propagation of the wetting front, leaving the soil at greater depths unaffected by the infiltrating rainfall for a longer time. This implies higher t_1 values, while t_2^* is not significantly affected by these changes. Furthermore, the lower conductivity associated to higher value of l, means that the accumulation of water content during the wetting front advancement is higher, and that translates into a higher degree of saturation of the apparent steady state conditions, S_P. The rate of change of the saturation degree for the downward wetting front propagation, i_1, is also strongly dependent on the l value: increasing values of l imply increasing values of i_1 for all the monitored points. In contrast, i_2 is not notably influenced by this parameter. Thus, the l parameter mainly influences the downwards advancement of the wetting front, whereas the Bottom-Up saturation is not clearly impacted by its changes.

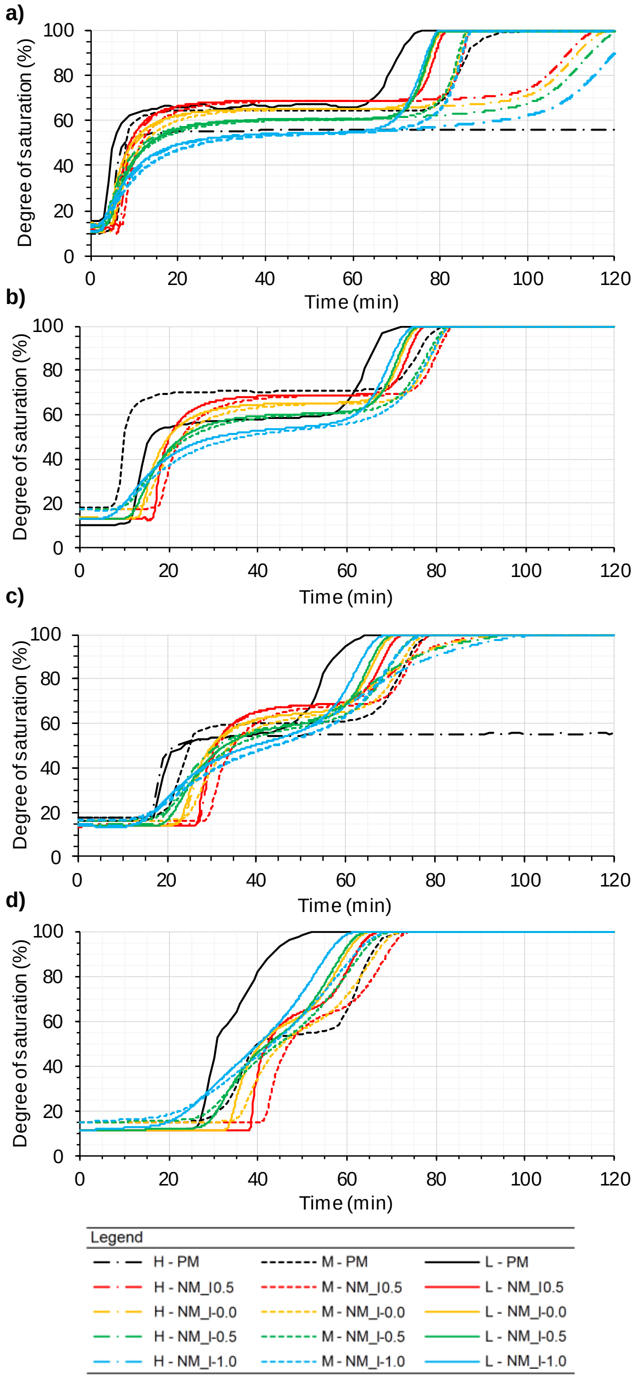

Fig. 11 Effect of the variation of the *l* parameter for the monitored points in the lower part (L, in continuous line), in the middle part (M, in dashed line), and in the upper part (H, in dot-dashed line) in terms of saturation degree at depths 6 cm (a), 12 cm (b), 18 cm (c), 24 cm (d) from ground level. [Legend: PM=Physical model, NM_xx=Numerical model case xx (see Table 3)]

Effect of parameter “$\mathbf{k_{sat}}$”

Fig. 12 shows the effect of the saturated hydraulic conductivity on the slope response in terms of saturation degree. Reasonably, this parameter is able to control both the downward wetting front advancement and Bottom-Up saturation mechanism. In particular, lower values of k_{sat} slow down the Bottom-Up saturation and the advancement of wetting front occurs at higher degrees of saturation. Particularly interesting is the case of the highest considered value of k_{sat}, which is able to simulate almost perfectly t_2^* for points L6, M12, L12, L18, L24, and to maintain point H6 into the apparent steady state conditions. However, in this case, the numerical values of $t_1$are slightly smaller than the physical ones. In terms of rate of changes, a lower k_{sat} provides higher values of both i_1 and i_2. Indeed, as $q/\,k_{sat}$ increases, the propagating wetting front tends to become closer to the Top-Down saturation described by the Green-Ampt model, and therefore the apparent steady state degree of saturation (S_P) increases and the variation of the saturation degree is also faster (increasing of i_1).

Both the l and k_{sat} parameters influence only the timing for the porewater pressure to reach the "plateau" and the final conditions, but they have no significant effect on the initial porewater pressure conditions.

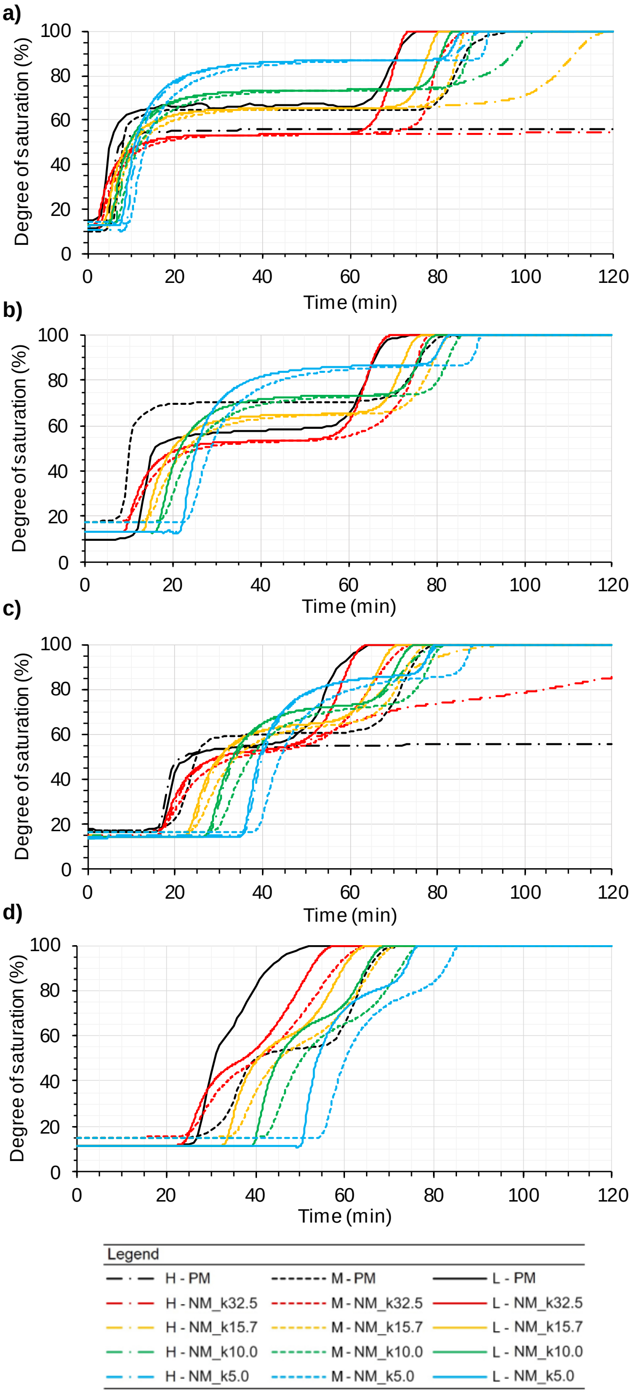

Fig. 12 Effect of the variation of the k_{sat} parameter for the monitored points in the lower part (L, in continuous line), in the middle part (M, in dashed line), and in the upper part (H, in dot-dashed line) in terms of saturation degree at depths 6 cm (a), 12 cm (b), 18 cm (c), 24 cm (d) from ground level. [Legend: PM=Physical model, NM_xx=Numerical model case xx (see Table 3)]

Best-fit simulation

According to what was described in the previous sections, once the contribution of each parameter to the hydraulic response of the slope is assessed, it is possible to use the experimentally obtained data to calibrate the numerical model and obtain the unsaturated hydraulic parameters of the investigated soil. To do so, a series of trial-and-error analyses were carried out. The best-fit simulation (NM_BestFit) is characterized by the set of parameters reported in Table 4.

Table 4 Set of best-fit hydraulic parameters for the optimized analysis of the case study

Parameter		NM_BestFit
S_r	(%)	5
S_{sat}	(%)	100
n	(-)	2.7
a	(kPa)	0.82
l	(-)	0.25
k_{sat}	(m/s)	$3.3 \cdot 10^{-4}$

The results of the analysis are shown in Fig. 13 and Fig. 14. Aside from a few discrepancies, the trends reported for the numerical model track the physical measurements adequately well. It is evident that the wetting front propagation and the Bottom-Up saturation timing (t_1 and t_2^*) are properly simulated. In addition, the average rate of change of the saturation degree for the Bottom-Up saturation (i_2) also agrees well with the physical evidence. The rate of change of the degree of saturation of the wetting front propagation (i_1) is slightly underestimated and, most notably, the S_P in the numerical model value is almost constant for all the points examined, differently from what is reported by the physical measurements. Given the homogeneous assumption adopted for the numerical model, the latter results are to be expected and, therefore, the fit for S_P at different depths and positions cannot be further improved by calibration in this model.

It should be noted that the accuracy of the calibrated model parameters is highly dependent on the suitability of the monitoring equipment to provide instantaneous data on the monitored variables in a given soil type. While there are sensors and measurement techniques that can cover a wide measurement range in fine-grained soils with low hydraulic conductivity, long equilibration times and slow response, as well as relatively low accuracy of the sensors when measuring in the wet range of the SWCC, may indicate seemingly slower changes in the monitored data and generally provide erroneous data sets for the calibration procedure. While the optimisation process is supported by the parametric analysis performed, consistency between the measured and calculated results should be ensured for multiple points throughout the domain and the parameters obtained should be checked for their soundness and representativeness for the soil material studied.

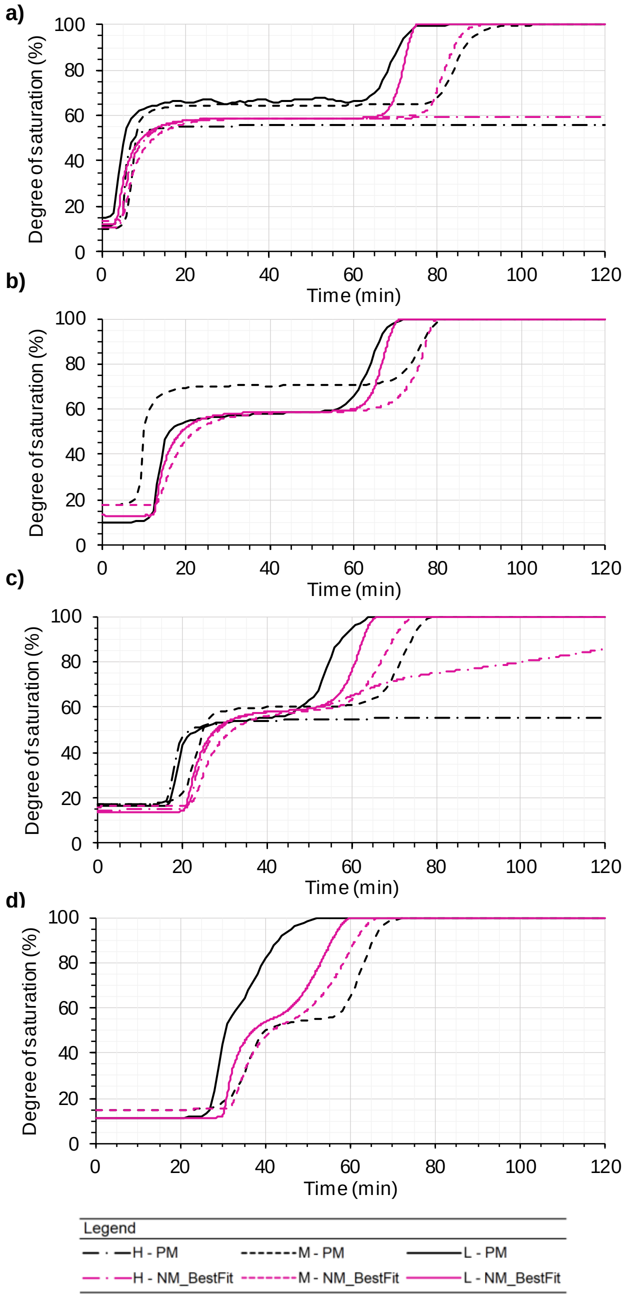

Fig. 13 Comparison of Best-Fit simulation (in pink) and measurements (in black) in correspondence of the monitored points in the lower part (L, in continuous line), in the middle part (M, in dashed line), and in the upper part (H, in dot-dashed line) in terms of the saturation degree at depths 6 cm (a), 12 cm (b), 18 cm (c), 24 cm (d) from the ground level

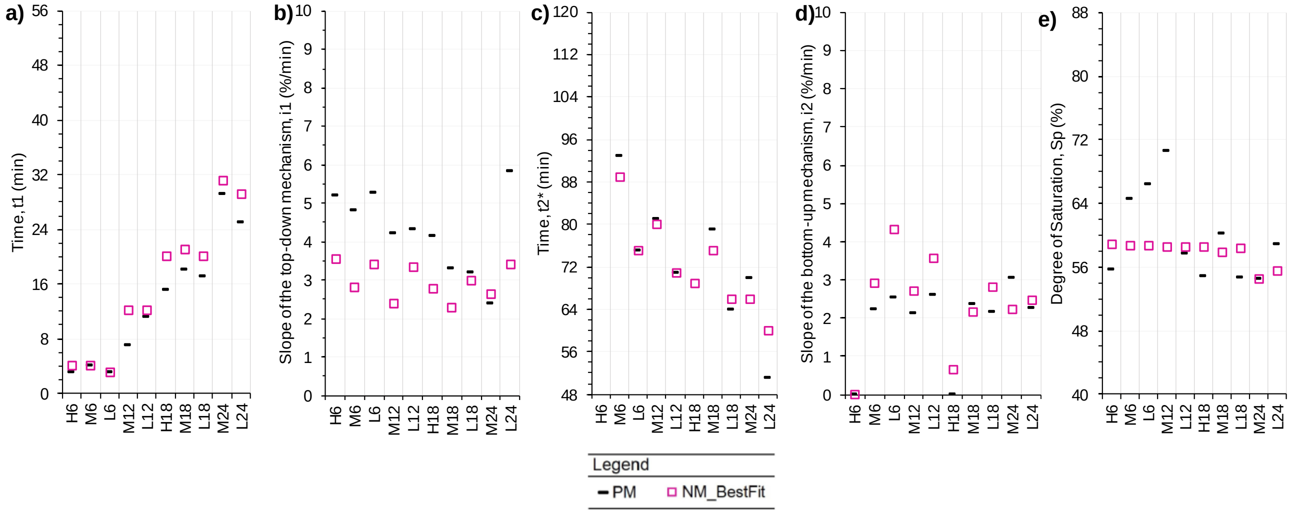

Fig. 14 Comparison of the optimized analysis (NM_BestFit, pink) with the physical measurements (PM, black) in the monitored points (see Fig. 3 for ID and location) for the following control parameters: a)t_1; b) i_1; c) t_2^*; d) i_2; e) S_p

Evaluating the performance of the numerical analysis

To evaluate the agreement between the numerical model results and the physical measurements, as well as to prove the validity of the procedure herein proposed and discussed, two different approaches have been considered. The first one assesses the errors between numerical and physical data in a standard way, as is most commonly done for time series comparison, adopting the following two global error metrics:

- Root Mean Square Error:

$$RMSE = \sqrt{\frac{1}{N} \cdot \sum_{i=1}^{N} (S_i^{NM} - S_i^{O})^2}$$

- Mean Prediction Error:

$$MPE = \frac{100\%}{N} \cdot \sum_{i=1}^{n} \frac{S_i^{NM} - S_i^{O}}{S_i^{O}}$$

where S_i^{NM} is the computed value of the degree of saturation at time t_i, S_i^{O} is the measured value of the degree of saturation at time t_i, and N is the number of points considered in the time series.

In a second approach, the errors between the numerical models and the physical observations are computed adopting five residual values, considering five of six key control parameters previously defined, as follows:

$$e(t_1) = t_1^{NM} - t_1^{O}$$

$$e(i_1) = i_1^{NM} - i_1^{O}$$

$$e(t_2^*) = t_2^{*NM} - t_2^{*O}$$

$$e(i_2) = i_2^{NM} - i_2^{O}$$

$$e(S_p) = S_p^{NM} - S_p^{O}$$

where the apex NM refers to the values of the control parameters in the numerical model and the apex O refers to the values of the control parameters in the observations.

Fig. 15 graphically depicts the meaning of these errors. In particular, the RMSE and MPE global metrics are related to the area comprised between the numerical results and the physical measurements time series, whereas the five adopted residual values represent the linear distance between the observed and the simulated values for t_1, t_2^*, and S_p, and the angular difference between the two values for i_1 and i_2.

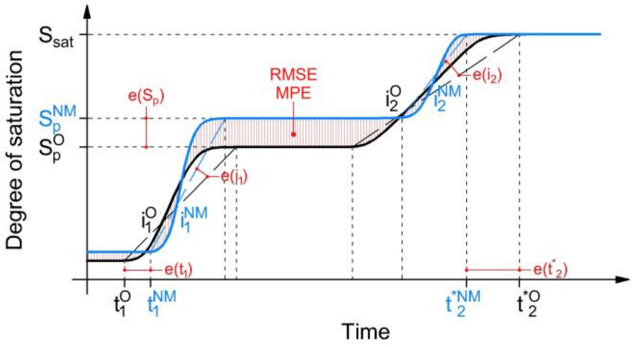

Fig. 15 Schematic comparison between the numerical results (in blue) and the physical monitoring (in black) in terms of degree of saturation time series, with a graphical representation of how the errors are considered in this study

Table 5 reports the values of the RMSE and MPE global error metrics for each monitored point and their average value (AVRG). Both indicators suggest a similar trend between the examined points, revealing that the model performs best at points H6 and L12 (i.e., RMSE equal to 3.26 and 3.72, and MPE equal to 3.64 and 0.66, respectively), while the worst performance is observed at points H18, M12 and L24. This is consistent with the evaluation carried out by means of the five residual values herein proposed (Table 6), which also indicates that points H6, L12, and M24 are the best simulated ones. Considering the single residuals, and their physical meaning: the shallowest points (i.e., H6, M6, L6, L12) show an almost perfect match with the wetting front arrival time, t_1; points L18 and M24 well relate to the duration of the wetting front advancement, represented by i_1; and points M18 and L24 are the ones showing the best modelling fit with the duration of the final saturation phase, related to the control parameter i_2. Good agreement between the numerical and physical models with respect to S_p was observed for all monitored points except for M12, for which an error of about 12% is computed.

Table 5 Global error metrics adopted for evaluating the performance of the models in terms of the degree of saturation data at different monitored points, also considering their average values (AVRG)

Metrix		H6	M6	L6	M12	L12	H18	M18	L18	M24	L24	AVRG
RMSE	(%)	3.26	6.08	7.75	14.10	3.72	17.27	6.58	7.75	5.66	13.00	8.52
MPE	(%)	3.64	-3.32	-9.24	-13.75	0.66	15.13	-3.57	-7.11	2.55	-9.15	-2.42

Table 6 Model performance evaluation by means of five residual values representative of five key control indicators related to the degree of saturation data at different monitoring points, also considering their average values (AVRG)

Metrix		H6	M6	L6	M12	L12	H18	M18	L18	M24	L24	AVRG
$e(t_1)$	(min)	1	0	0	5	1	5	3	3	2	4	2.40
$e(i_1)$	(%/min)	-1.65	-1.99	-1.86	-1.86	-0.99	-1.38	-1.00	-0.20	0.22	-2.44	-1.32
$e(t_2^*)$	(min)	-	-4	0	-1	0	-	-4	2	-4	9	-0.25
$e(i_2)$	(%/min)	-	0.71	1.75	0.60	0.95	-	-0.21	0.63	-0.85	0.20	0.47
$e(S_p)$	(%)	3.18	-6.00	-7.69	-12.09	0.85	3.71	-2.39	3.67	-0.05	-3.30	-2.01

Finally, the average values of the five residuals are compared in Fig. 16 for all the analyses considered. As it is clearly visible, the range of errors is mostly contained within a relatively small range of values, even though significant residuals are computed for the analyses NM_n2.1, NM_k4.3, and NM_k8.6. Although the best fit model seems to be similar to NM_n3.9 and NM_n4.8, these three models are considerably different in the topmost part of the slope (H), where only the NM_BestFit model does not reach the fully saturated conditions (in agreement with the physical measurements).

NM_	BC	a2.0	a0.7	a0.5	n2.1	n3.9	n4.8	l-1.0	l-5.0	l0.5	k5.0	k10.0	k32.5	BestFit
■ e(t1) (min)	3.90	0.10	5.80	6.80	10.00	2.40	1.30	-3.90	-0.10	7.90	14.70	7.70	-1.70	2.40
■ e(i1) (%/min)	-1.59	-2.27	-0.96	-0.35	-1.44	-1.55	-1.39	-2.82	-2.25	-0.83	-0.98	-1.39	-1.89	-1.32
■ e(t*2) (min)	3.50	7.00	2.13	1.25	9.25	1.13	-1.38	2.00	2.50	5.00	12.25	7.25	-2.25	-0.25
■ e(i2) (%/min)	0.20	-0.72	1.02	1.91	0.00	0.55	0.87	-0.15	0.08	0.33	0.26	0.18	0.23	0.47
■ e(Sp) (%)	3.61	-0.28	4.67	5.10	14.30	-1.88	-5.22	-8.70	-1.87	7.81	24.53	11.55	-7.79	-2.01

Fig. 16 Average residual error values for the different cases of parametric analysis and for the best-fit model

Conclusions

A new methodological approach has been proposed to calibrate the unsaturated hydraulic properties of a coarse-grained soil undergoing a wetting process, using water content measurements on a well-monitored physical model of a slope subjected to constant rainfall infiltration. The soil considered in the study has negligible volumetric deformations when subjected a wetting process, and thus the interpretation of the experimental results justifies the use of an uncoupled numerical modelling approach. The procedure is built around the wetting front concept and uses six control parameters to guide the trial-and-error calibration of the numerical model of the slope. In particular, the first derivative of the evolution over time of the degree of saturation is used to define, objectively by means a properly set threshold value, the key times of the infiltration process in the locations where monitoring data are available. Unlike more traditional error evaluation methodologies, the proposed approach focuses on the peculiar characteristics of the rainfall infiltration and soil saturation mechanisms, to effectively guide the calibration procedure from a geotechnical point of view. The validity of the outcome of the calibration has been also verified adopting standard time-series error metrics, i.e., comparing the time-dependent degree of saturation measures in the different monitored points with the corresponding model results. In conclusion, this study clearly highlighted and quantified the significant influence of SWCC and HFC in controlling the soil response in a slope subjected to constant and prolonged rainfall infiltration.

Acknowledgements

This research was funded by the Croatian Science Foundation under the Project IP-2018-1503 Physical modelling of landslide remediation constructions behaviour under static and seismic actions (ModLandRemSS). The part of the laboratory equipment used for laboratory testing was provided in the frame of the project Research Infrastructure for Campus-based Laboratories at the University of Rijeka, co-funded in a part by the Ministry of Science, Education, and Sports of the Republic of Croatia and the European Regional Development Fund (ERDF). This work has been supported by the International Consortium on Landslides under the IPL-256 and IPL-265 projects. This work has been partially supported by the University of Rijeka project uniri-mladi-tehnic-22-62. These supports are gratefully acknowledged.

Data availability statement

The datasets generated during and/or analysed during the current study are available from the corresponding author on reasonable request.

Declarations

The authors have no relevant financial or non-financial interests to disclose. The authors declare no conflict of interest. The funders had no role in the design of the study; in the collection, analyses, or interpretation of data; in the writing of the manuscript, or in the decision to publish the results.

References

1. Ali S, Ghosh NC (2015) Methodology for the Estimation of Wetting Front Length and Potential Recharge under Variable Depth of Ponding. Journal of Irrigation and Drainage Engineering 142:04015027. https://doi.org/10.1061/(ASCE)IR.1943-4774.0000921

2. Angeli MG, Buma J, Gasparetto P, Pasuto A (1998) A combined hillslope hydrology/stability model for low-gradient clay slopes in the Italian Dolomites. Eng Geol 49:1–13. https://doi.org/10.1016/S0013-7952(97)00033-1

3. Benson CH, Chiang I, Chalermyanont T, Sawangsuriya A (2014) Estimating van Genuchten Parameters α and n for Clean Sands from Particle Size Distribution Data. 410–427. https://doi.org/10.1061/9780784413265.033

4. Bordoni M, Meisina C, Valentino R, et al (2015) Hydrological factors affecting rainfall-induced shallow landslides: From the field monitoring to a simplified slope stability analysis. Eng Geol 193:19–37. https://doi.org/10.1016/J.ENGGEO.2015.04.006

5. Brinkgreve RBJ, Kumarswamy S, Swolfs WM (2016) PLAXIS 2D 2016 Manuals. PLAXIS 2016

6. Brönnimann CS (2011) Effect of Groundwater on Landslide Triggering. https://doi.org/10.5075/EPFL-THESIS-5236

7. Brooks RH (1965) Hydraulic properties of porous media. Colorado State University

8. Burdine NT (1953) Relative Permeability Calculations From Pore Size Distribution Data. Journal of Petroleum Technology 5:71–78. https://doi.org/10.2118/225-G

9. Carey JM, Moore R, Petley DN (2015) Patterns of movement in the Ventnor landslide complex, Isle of Wight, southern England. Landslides 12:1107–1118. https://doi.org/10.1007/S10346-014-0538-1/FIGURES/13

10. Cascini L, Calvello M, Grimaldi GM (2010) Groundwater Modeling for the Analysis of Active Slow-Moving Landslides. Journal of Geotechnical and Geoenvironmental Engineering 136:1220–1230. https://doi.org/10.1061/(ASCE)GT.1943-5606.0000323

11. Cascini L, Cuomo S, Pastor M, Sorbino G (2009) Modeling of Rainfall-Induced Shallow Landslides of the Flow-Type. Journal of Geotechnical and Geoenvironmental Engineering 136:85–98. https://doi.org/10.1061/(ASCE)GT.1943-5606.0000182

12. Chae BG, Kim M Il (2012) Suggestion of a method for landslide early warning using the change in the volumetric water content gradient due to rainfall infiltration. Environ Earth Sci 66:1973–1986. https://doi.org/10.1007/S12665-011-1423-Z/FIGURES/8

13. Chen G, Meng X, Qiao L, et al (2018) Response of a loess landslide to rainfall: observations from a field artificial rainfall experiment in Bailong River Basin, China. Landslides 15:895–911. https://doi.org/10.1007/S10346-017-0924-6/TABLES/4

14. Childs EC, Bybordi M (1969) The vertical movement water in stratified porous material: 1. Infiltration. Water Resour Res 5:446–459. https://doi.org/10.1029/WR005I002P00446

15. Chu X, Mariño MA (2005) Determination of ponding condition and infiltration into layered soils under unsteady rainfall. J Hydrol (Amst) 313:195–207. https://doi.org/10.1016/J.JHYDROL.2005.03.002

16. Coe JA, Ellis WL, Godt JW, et al (2003) Seasonal movement of the Slumgullion landslide determined from Global Positioning System surveys and field instrumentation, July 1998–March 2002. Eng Geol 68:67–101. https://doi.org/10.1016/S0013-7952(02)00199-0

17. Corsini A, Pasuto A, Soldati M, Zannoni A (2005) Field monitoring of the Corvara landslide (Dolomites, Italy) and its relevance for hazard assessment. Geomorphology 66:149–165. https://doi.org/10.1016/J.GEOMORPH.2004.09.012

18. Cresswell HP, Green TW, McKenzie NJ (2008) The Adequacy of Pressure Plate Apparatus for Determining Soil Water Retention. Soil Science Society of America Journal 72:41–49. https://doi.org/10.2136/SSSAJ2006.0182

19. Cui YJ, Tang AM, Loiseau C, Delage P (2008) Determining the unsaturated hydraulic conductivity of a compacted sand–bentonite mixture under constant-volume and free-swell conditions. Physics and Chemistry of the Earth, Parts A/B/C 33:S462–S471. https://doi.org/10.1016/J.PCE.2008.10.017

20. Deng P, Zhu J (2016) Analysis of effective Green–Ampt hydraulic parameters for vertically layered soils. J Hydrol (Amst) 538:705–712. https://doi.org/10.1016/J.JHYDROL.2016.04.059

21. Eching SO, Hopmans JW (1993) Optimization of Hydraulic Functions from Transient Outflow and Soil Water Pressure Data. Soil Science Society of America Journal 57:1167–1175. https://doi.org/10.2136/SSSAJ1993.03615995005700050001X

22. Editors A, Ku C-Y, Tsai F, et al (2022) The Key Parameters Involved in a Rainfall-Triggered Landslide. Water 2022, Vol 14, Page 3561 14:3561. https://doi.org/10.3390/W14213561

23. Farrell DA, Larson WE (1972) Modeling the pore structure of porous media. Water Resour Res 8:699–706. https://doi.org/10.1029/WR008I003P00699

24. Fatt I, Dykstra H (1951) Relative Permeability Studies. Journal of Petroleum Technology 3:249–256. https://doi.org/10.2118/951249-G

25. Finnegan NJ, Perkins JP, Nereson AL, Handwerger AL (2021) Unsaturated Flow Processes and the Onset of Seasonal Deformation in Slow-Moving Landslides. J Geophys Res Earth Surf 126:e2020JF005758. https://doi.org/10.1029/2020JF005758

26. Fredlund DG, Anqing Xing (2011) Equations for the soil-water characteristic curve. https://doi.org/101139/t94-061 31:521–532. https://doi.org/10.1139/T94-061

27. Freyberg DL, Reeder JW, Franzini JB, Remson I (1980) Application of the Green-Ampt Model to infiltration under time-dependent surface water depths. Water Resour Res 16:517–528. https://doi.org/10.1029/WR016I003P00517

28. Gaspar TA V, Jacobsz SW, Schultz-Poblete M, Toll DG (2019) Measurement of the soil water retention curve: practical considerations. In: Proceedings of the 17th African Regional Conference on Soil Mechanics and Geotechnical Engineering, SAICE. pp 7–9

29. Gee GW, Ward AL, Zhang ZF, et al (2002) The Influence of Hydraulic Nonequilibrium on Pressure Plate Data. Vadose Zone Journal 1:172–178. https://doi.org/10.2113/1.1.172

30. Genuchten MTh van (1980) A Closed-form Equation for Predicting the Hydraulic Conductivity of Unsaturated Soils. Soil Science Society of America Journal 44:892–898. https://doi.org/10.2136/SSSAJ1980.03615995004400050002X

31. Ghanbarian-Alavijeh B, Liaghat A, Huang GH, Van Genuchten MT (2010) Estimation of the van Genuchten Soil Water Retention Properties from Soil Textural Data. Pedosphere 20:456–465. https://doi.org/10.1016/S1002-0160(10)60035-5

32. Hazen A (1983) Some Physical properties of sand and gravel with special reference to their use in filtration. Boston

33. Heber Green W, Ampt GA (1911) Studies on Soil Phyics. J Agric Sci 4:1–24. https://doi.org/10.1017/S0021859600001441

34. Hong Y, Hiura H, Shino K, et al (2005) Quantitative assessment on the influence of heavy rainfall on the crystalline schist landslide by monitoring system -case study on Zentoku landslide, Japan. Landslides 2:31–41. https://doi.org/10.1007/S10346-005-0044-6/FIGURES/11

35. Huat BBK, Prasad Arun, Toll DG (2012) Handbook of tropical residual soils engineering. 532

36. Inoue M, Šimunek J, Hopmans JW, Clausnitzer V (1998) In situ estimation of soil hydraulic functions using a multistep soil-water extraction technique. Water Resour Res 34:1035–1050. https://doi.org/10.1029/98WR00295

37. Kuang X, Jiao JJ (2011) A new model for predicting relative nonwetting phase permeability from soil water retention curves. Water Resour Res 47:8520. https://doi.org/10.1029/2011WR010728

38. Kumar Dahal R, Hasegawa S, Yamanaka M, Nishino K (2006) Rainfall triggered flow-like landslides: Understanding from southern hills of Kathmandu, Nepal and Northern Shikoku, Japan

39. Ladd RS (1974) Specimen Preparation and Liquefaction of Sands. Journal of the Geotechnical Engineering Division 100:1180–1184. https://doi.org/10.1061/AJGEB6.0000117

40. Lee K, Suk J, Kim H, Jeong S (2021) Modeling of rainfall-induced landslides using a full-scale flume test. Landslides 18:1153–1162. https://doi.org/10.1007/S10346-020-01563-8/FIGURES/10

41. Leng Y, Peng J, Wang Q, et al (2018) A fluidized landslide occurred in the Loess Plateau: A study on loess landslide in South Jingyang tableland. Eng Geol 236:129–136. https://doi.org/10.1016/J.ENGGEO.2017.05.006

42. Leong EC, Rahardjo H (1997) Review of Soil-Water Characteristic Curve Equations. Journal of Geotechnical and Geoenvironmental Engineering 123:1106–1117. https://doi.org/10.1061/(ASCE)1090-0241(1997)123:12(1106)

43. Leong EC, Tripathy S, Rahardjo H (2004) A Modified Pressure Plate Apparatus. Geotechnical Testing Journal 27:322–331. https://doi.org/10.1520/GTJ11053

44. Lissak C, Maquaire O, Malet JP, Davidson R (2014) Piezometric thresholds for triggering landslides along the Normandy coast, France. http://journals.openedition.org/geomorphologie 145–158. https://doi.org/10.4000/GEOMORPHOLOGIE.10607

45. Liu G, Tong F guo, Zhao Y tong, Tian B (2018) A force transfer mechanism for triggering landslides during rainfall infiltration. J Mt Sci 15:2480–2491. https://doi.org/10.1007/S11629-018-5043-X/METRICS

46. Liu HD, Li DD, Wang ZF, et al (2020) Physical modeling on failure mechanism of locked-segment landslides triggered by heavy precipitation. Landslides 17:459–469. https://doi.org/10.1007/S10346-019-01288-3/FIGURES/13

47. Malet JP, Maquaire O, Calais E (2002) The use of Global Positioning System techniques for the continuous monitoring of landslides: application to the Super-Sauze earthflow (Alpes-de-Haute-Provence, France). Geomorphology 43:33–54. https://doi.org/10.1016/S0169-555X(01)00098-8

48. Marinho FAM, Take WA, Tarantino A (2009) Measurement of matric suction using tensiometric and axis translation techniques. Laboratory and Field Testing of Unsaturated Soils 3–19. https://doi.org/10.1007/978-1-4020-8819-3_2/COVER

49. Massey CI, Petley DN, McSaveney MJ (2013) Patterns of movement in reactivated landslides. Eng Geol 159:1–19. https://doi.org/10.1016/J.ENGGEO.2013.03.011

50. Moriwaki H, Inokuchi T, Hattanji T, et al (2004) Failure processes in a full-scale landslide experiment using a rainfall simulator. Landslides 1:277–288. https://doi.org/10.1007/S10346-004-0034-0/FIGURES/21

51. Mualem Y (1976) A new model for predicting the hydraulic conductivity of unsaturated porous media. Water Resour Res 12:513–522. https://doi.org/10.1029/WR012I003P00513

52. Nakhaei M, Šimůnek J (2014) Parameter estimation of soil hydraulic and thermal property functions for unsaturated porous media using the HYDRUS-2D code. Journal of Hydrology and Hydromechanics 62:7–15. https://doi.org/10.2478/JOHH-2014-0008

53. Olivares L, Damiano E, Greco R, et al (2009) An Instrumented Flume to Investigate the Mechanics of Rainfall-Induced Landslides in Unsaturated Granular Soils

54. Oliveira OM, Fernando FAM (2006) Study of Equilibration Time in the Pressure Plate. 1864–1874. https://doi.org/10.1061/40802(189)157

55. Pajalić S, Peranić J, Maksimović S, et al (2021) Monitoring and Data Analysis in Small-Scale Landslide Physical Model. Applied Sciences 2021, Vol 11, Page 5040 11:5040. https://doi.org/10.3390/APP11115040

56. Peranić J, Arbanas Ž, Cuomo S, Maček M (2018) Soil-water characteristic curve of residual soil from a flysch rock mass. Geofluids 2018:. https://doi.org/10.1155/2018/6297819

57. Peranić J, Čeh N, Arbanas Ž (2022) The Use of Soil Moisture and Pore-Water Pressure Sensors for the Interpretation of Landslide Behavior in Small-Scale Physical Models. Sensors 2022, Vol 22, Page 7337 22:7337. https://doi.org/10.3390/S22197337

58. Peranić J, Mihalić Arbanas S, Arbanas Ž (2021) Importance of the unsaturated zone in landslide reactivation on flysch slopes: observations from Valići Landslide, Croatia. Landslides 18:3737–3751. https://doi.org/10.1007/S10346-021-01757-8/FIGURES/18

59. Peranić J, Moscariello M, Cuomo S, Arbanas Ž (2020) Hydro-mechanical properties of unsaturated residual soil from a flysch rock mass. Eng Geol 269:105546. https://doi.org/10.1016/J.ENGGEO.2020.105546

60. Rahardjo H, Ong TH, Rezaur RB, Leong EC (2007) Factors Controlling Instability of Homogeneous Soil Slopes under Rainfall. Journal of Geotechnical and Geoenvironmental Engineering 133:1532–1543. https://doi.org/10.1061/(ASCE)1090-0241(2007)133:12(1532)/ASSET/DB98B9BA-52B5-43E1-BF2C-BD0376F9ACB1/ASSETS/IMAGES/LARGE/10.JPG

61. Ren Y, Li T, Dong S, et al (2020) Rainfall-induced reactivation mechanism of a landslide with multiple-soft layers. Landslides 17:1269–1281. https://doi.org/10.1007/S10346-020-01357-Y/FIGURES/14

62. Richards LA (2004) Capillary conduction of liquids through porous mediums. Physics (College Park Md) 1:318. https://doi.org/10.1063/1.1745010

63. Ridley AM, Burland JB (1993) A new instrument for the measurement of soil moisture suction. 43:321–324

64. Schaap MG, Leij FJ (2000) Improved Prediction of Unsaturated Hydraulic Conductivity with the Mualem-van Genuchten Model. Soil Science Society of America Journal 64:843–851. https://doi.org/10.2136/SSSAJ2000.643843X

65. Šimunek J, van Genuchten MT (1996) Parameter estimation of soil hydraulic properties from the tension disc infiltrometer experiment by numerical inversion. Water Resour Res 32:2683–2696

66. Šimůnek J, Van Genuchten MT, Gribb MM, Hopmans JW (1998) Parameter estimation of unsaturated soil hydraulic properties from transient flow processes. Soil Tillage Res 47:27–36. https://doi.org/10.1016/S0167-1987(98)00069-5

67. Sun H, Wong H, Ho K (1998) Analysis of infiltration in unsaturated ground. In... - Google Scholar. In: Proceedings of the annual seminar on slope engineering in Hong Kong. pp 101–109

68. Take WA, Beddoe RA, Davoodi-Bilesavar R, Phillips R (2015) Effect of antecedent groundwater conditions on the triggering of static liquefaction landslides. Landslides 12:469–479. https://doi.org/10.1007/S10346-014-0496-7/FIGURES/14

69. Tohari A, Nishigaki M, Komatsu M (2007) Laboratory Rainfall-Induced Slope Failure with Moisture Content Measurement. Journal of Geotechnical and Geoenvironmental Engineering 133:575–587. https://doi.org/10.1061/(ASCE)1090-0241(2007)133:5(575)

70. Tsaparas I, Rahardjo H, Toll DG, Leong EC (2002) Controlling parameters for rainfall-induced landslides. Comput Geotech 29:1–27. https://doi.org/10.1016/S0266-352X(01)00019-2

71. Tu XB, Kwong AKL, Dai FC, et al (2009) Field monitoring of rainfall infiltration in a loess slope and analysis of failure mechanism of rainfall-induced landslides. Eng Geol 105:134–150. https://doi.org/10.1016/J.ENGGEO.2008.11.011

72. Tuller M, Or D (2005) Water retention and characteristic curve. Encyclopedia of Soils in the Environment 4:278–289. https://doi.org/10.1016/B0-12-348530-4/00376-3

73. Wang G, Sassa K (2003) Pore-pressure generation and movement of rainfall-induced landslides: effects of grain size and fine-particle content. Eng Geol 69:109–125. https://doi.org/10.1016/S0013-7952(02)00268-5

74. Wayllace A, Lu N (2012) A Transient Water Release and Imbibitions Method for Rapidly Measuring Wetting and Drying Soil Water Retention and Hydraulic Conductivity Functions

75. Williams J, Prebble RE, Williams WT, Hignett CT (1983) The influence of texture, structure and clay mineralogy on the soil moisture characteristic. Soil Research 21:15–32. https://doi.org/10.1071/SR9830015

76. Yang C, Sheng D, Carter JP (2012) Effect of hydraulic hysteresis on seepage analysis for unsaturated soils. Comput Geotech 41:36–56. https://doi.org/10.1016/J.COMPGEO.2011.11.006

77. Zhang X, Mavroulidou M, Gunn MJ (2017) A study of the water retention curve of lime-treated London Clay. Acta Geotech 12:23–45. https://doi.org/10.1007/S11440-015-0432-6/TABLES/9

Appendix A. List of symbols

Symbol	Description
a	Van Genuchten parameter
C_c	Capillarity coefficient
CU	Uniformity coefficient
D_{10}	Particle diameter corresponding to 10% cumulative undersize particle size distribution
D_{60}	Particle diameter corresponding to 60% cumulative undersize particle size distribution
d	Rainfall duration
$D_{r,i}$	Initial relative density
$e(x)$	Residual error of the control parameter x
e_{max}	Maximum void ratio
e_{min}	Minimum void ratio
G_s	Specific gravity
h	Ponding head
h_p	Ponding head
i_1	Rate of change of saturation degree for downward wetting front propagation
i_2	Rate of change of saturation degree for bottom-up saturation
k_{sat}	Saturated hydraulic conductivity
l	Hydraulic conductivity function parameter
m	Van Genuchten parameter
n	Van Genuchten parameter
n_s	Soil porosity
$n_{s,i}$	Initial soil porosity
q	Rainfall intensity
q_0	Surface flux at steady state conditions
q_1	Surface flux under transient conditions
S	Degree of saturation
S'	First derivative of the degree of saturation
S_0	Initial degree of saturation
S_e	Effective degree of saturation
S_{in}	Degree of saturation below the wetting front
S_P	Degree of saturation for the apparent steady state conditions
S_{q_0}	Degree of saturation at q_0
S_{q_1}	Degree of saturation at q_1
S_r	Residual deree of saturation
S_{sat}	Degree of saturation at fully saturated state
t^*	Time of abruptly changing of degree of saturation
t_1	Time of initial change in saturation degree
t_2^*	Time of fully saturated conditions

Symbol	Description
t_{sat}	Saturation time
w_i	Initial gravimetric water content
z_{sat}	Depth of the saturation front
z_w	Depth of the wetting front

Appendix B. List of abbreviations

Abbreviation	Description
$AVRG$	Average value
HFC	Hydraulic Conductivity Function
MPE	Mean Predicted Error
N	Number of observations
NM	Numerical Model
PM	Physical Model
$RMSE$	Root Mean Square Error
ST	Schematic Trend
$SWCC$	Soil Water Characteristic Curve
TS	Threshold value